EES Batteries

ROYAL SOCIETY OF CHEMISTRY

ANALYSIS

View Article Online
View Journal

Cite this: DOI: 10.1039/d5eb00161g

Initial characterization and cycling of two batches of commercial hard-carbon/$Na_xNi_yFe_zMn_{1-y-z}O_2$ sodium ion 18650 batteries as a potential replacement for lithium-ion batteries

R. M. Wittman, *[a] D. Anseán, *[b] M. L. Meyerson,[c] D. Beck,[d] E. E. Valdés,[b] V. M. García,[e] I. Cameán,[f] C. Rich,[g] J. Langendorf,[g] M. Rodriguez,[c] N. Valdez,[c] J. Román-Kustas,[h] D. Schafer,[h] B. Juba,[h] A. Bates,[g] L. Torres-Castro[g] and M. Dubarry *[d]

Received 5th September 2025,
Accepted 30th October 2025

DOI: 10.1039/d5eb00161g

rsc.li/EESBatteries

This work presents a comparative analysis of two initial release commercial sodium-ion 18650 cells manufactured by Tycorun and Hakadi with identical layered oxide ($NaNi_{1/3}Fe_{1/3}Mn_{1/3}O_2$) cathodes and hard carbon anodes. Through electrochemical benchmarking and advanced materials characterization, this study evaluated cell-to-cell variability, interfacial chemistry, and early-life degradation pathways. Both batches demonstrated manufacturing consistency analogous to lithium-ion standards but differences in binder type and electrolyte formulation which induced distinct solid electrolyte interphase characteristics. Overall, capacity retention fell significantly short of manufacturer specifications, with observable failure modes in Hakadi cells linked to a wider operating voltage window. These findings underscore the need for standardization in manufactured components, operating parameters, and in initial cell testing to evaluate performance.

Broader context

In recent years, Na-ion batteries have been rapidly developed and introduced to the commercial market. However, there is limited information regarding the quality of the initial cells produced, the materials and manufacturing processes used, the consistency of these cells, and their optimal use cases. This information is critical for potential end users and anyone interacting with these products in real-world applications. In this work, we aim to address some of these gaps by providing a side-by-side comparison of two different Na-ion batteries purchased from distinct manufacturers. Our findings indicate that these cells broadly utilize the same electrode materials, with notable differences in binder and electrolyte composition. The cells demonstrate batch consistency comparable to that of Li-ion batteries, suggesting that the manufacturing processes for Li-ion batteries can be relatively easily adapted for Na-ion batteries within this material class. However, both cells exhibit only about 10% of the rated cycle life specified by the manufacturers, which may be attributed to variations in materials or operating conditions. This suggests that further work is needed to enhance the viability of Na-ion cells on a commercial scale.

Introduction

In recent years, commercial sodium-ion batteries (NIBs) have started to become available as a possible replacement for lithium-ion batteries (LIBs). Many different configurations of NIBs are being pursued,[1,2] with some having performance characteristics approaching the needs of grid energy storage and vehicle electrification applications[3,4] and show promise for better power, cyclability, safety, recyclability, and cost[3,5,6] than their Li-ion counterparts. Rudola *et al.*[7] provided a brief history of NIBs, and some literature on the testing of commercial NIBs has started to emerge on prototype[8–10] or commercial cells.[7,11–16] This includes work on cells from Faradion,[7] Natron,[11] Tiamat,[12,13] Shenzhen Mushang Electronics,[14,16] and

[a]Energy Storage Technology and Systems, Sandia National Laboratories, Albuquerque, New Mexico, USA. E-mail: rwittm@sandia.gov
[b]Department of Electrical Engineering, Polytechnic School of Engineering, University of Oviedo, Gijón, Asturias, Spain. E-mail: anseandavid@uniovi.es
[c]Materials Characterization and Performance, Sandia National Laboratories, Albuquerque, New Mexico, USA
[d]Hawaii Natural Energy Institute, University of Hawaii at Manoa, Honolulu, HI, USA. E-mail: matthieu@hawaii.edu
[e]Department of Physical and Analytical Chemistry, Polytechnic School of Engineering, University of Oviedo, Gijón, Asturias, Spain
[f]Instituto de Ciencia y Tecnología del Carbono, INCAR-CSIC, Oviedo, Spain
[g]Power Sources R&D, Sandia National Laboratories, Albuquerque, New Mexico, USA
[h]Analytical Science & Corrosion, Sandia National Laboratories, Albuquerque, New Mexico, USA

Hakadi[15] that used different electrode material such as layered oxides, polyanion, or Prussian blue analogues for the positive electrode (PE), and hard carbons (HC) or Prussian blue analogues for the negative electrode (NE).

Layered oxides were the first PE material commercialized for NIBs. Their primary drawbacks compared to Prussian blue and fluorophosphates are typically their lower cyclability and higher material cost from elements like Ni and Co. Among the proposed oxides, $Na_xNi_yFe_zMn_{1-y-z}O_2$ (NFM) mitigated the cost issues by omitting Co from the composition. It also demonstrated an acceptable cycle life, ~1500 equivalent full cycles with 85% capacity remaining,[14,17] offered relatively high capacity, ~190 mAh g^{-1}, and ease of manufacturing.[18]

The use of NFM as the PE for NIBs was initially proposed by Kim *et al.* from the Argonne National Laboratory who found that it could be charged up to 4 V without irreversible phase transitions.[19] They identified the crystal structure as belonging to the $R\bar{3}m$ space group, specifically indexed to the α-$NaFeO_2$ structure. This is very similar to the metal oxides commonly used for LIBs, such as nickel, cobalt, manganese, and aluminum oxides. Kim *et al.* found that the NFM material could be cycled 150 times without significant changes to its crystal structure. Work by Duffort *et al.* showed that when charging the material to 4.3 V, there was a transition that would indicate a change in the insertion/desertion process of the Na^+ ions.[20] Xie *et al.* studied the crystal structure of NFM(111) material during charge and discharge[21] and found that charging to 4.3 V introduced a new phase with a monoclinic structure. This suggested an upper voltage limit for the NFM-based cells near 4 V before an irreversible degradation occurred.

Looking at the NE, the primary choice for NIBs is hard carbon (HC). It combines graphitic and amorphous carbon domains and accommodates Na^+ ions through intercalation and other storage mechanisms such as adsorption and pore filling.[2,7,10] It shows relatively stable cycle life 1000 or more cycles depending on cycling conditions and reasonable capacities of 300–350 mAh g^{-1}.[22–25] The preferred structure of HC in the NE is still being determined[2,26–29] and the intercalation process for Na^+ ions is still not well understood, with six different potential mechanisms proposed.[23] This also leads to uncertainty about preferred particle and pore size and the optimal ratio of graphitic to amorphous carbon for operation.[22] This is further complicated by unknowns about the composition of the solid electrolyte interphase (SEI) depending on HC and electrolyte properties.[30]

Most electrolytes for NIBs currently use a combination of organic solvents typically seen in LIB, and analogous Na salts (*e.g.* $NaPF_6$).[14,30] Similar to LiBs, the electrolyte in NIBs forms an SEI layer on the NE and a corresponding cathode electrolyte interphase on the PE.[31] Both these interphases are crucial in dictating Na^+ transport to and from the electrodes. As with LIBs, the composition of the electrolyte determines how these layers are formed, their stability, and the rate at which they grow during operation.

Previous literature with NFM-based NIB testing suggested they might be able to drop into LIB applications with relative ease.[14,15] However, to ascertain commercial viability, the variance in manufactured cells and the impact on battery operation across manufacturers must be evaluated.

In this work, two batches of commercial NIBs from Tycorun (TCR) and Hakadi (HKD) were studied. Both manufacturers use a similar chemistry consisting of NFM for the PE and HC for the NE. This is similar to the chemistry presented by Bischof *et al.*,[15] that also studied the HKD cells, and by Laufen *et al.*, who studied cells from Shenzhen Mushang Electronics.[14,16] A subset of cells from each batch was subjected to an initial conditioning and reference performance test (RPT) to assess cell-to-cell variations. This was followed by extensive material characterization on both cell chemistries. Finally, cells were cycled to observe initial performance.

Our results show that both types of cells have similar PEs, and small but distinct differences in the NEs and electrolyte. However, the cycle life appears to be more strongly affected by the voltage cutoff than these construction differences. Initial cycling data for each chemistry showcased a much shorter life than advertised or reported in the literature.

Results and discussion

Cell-to-cell variations

The assessment of cell-to-cell variations is a crucial step when testing new batches of commercial cells.[32,33] This assessment allows for the quantification of how consistent the manufacturing process is at producing quality cells reproducibly. Cell-to-cell variations have significant impact on cycleability when assembling cells into modules, where the weakest-performing cell will limit the performance of the whole module and provide pathways for asymmetric degradation.[34] Cell batches can be characterized by maximum capacity, rate capability, and resistance[33] as these three attributes describe the entire capacity *vs.* rate relationship.[35] In addition, checking the electrochemical response at low rates allows for assessing cell reaction reproducibility.[36] The results of the cell-to-cell variations analysis for 20 TCR cells and 20 HKD cells are presented in Fig. 1. As anticipated from the manufacturer's data sheet, the TCR cells had, on average, a slightly lower capacity than the HKD cells, 1.450 Ah *vs.* 1.579 Ah, Fig. 1(a and b). Both cells were tested to an upper voltage limit of 4.10 V for the initial RPT testing, so the difference in capacity observed is not due to a difference in the voltage limit.

Still, both cells had similar standard deviations in capacity (0.69% to 1.03%), as well as similar average rate capabilities (98.7 *vs.* 98.3, calculated as the ratio of the C/2 and C/4.5 capacities), and normalized resistances (151 *vs.* 159 mΩ Ah, calculated from the IR drop from the C/2 discharges). Still, the spread was larger for the HKD cells compared to the TCR cells (0.2% *vs.* 0.1% and 38 *vs.* 22 mΩ Ah, respectively). Overall, the cell-to-cell variations were comparable to Li-ion cells. When summarized on a 3D plot, Fig. 1(c and d), it can be seen that all but three cells were within 1σ for the TCR cells (all within 2σ) and all but 1 for the HKD cells, with one cell having a much higher resistance outside of 2σ. Notably, the observed

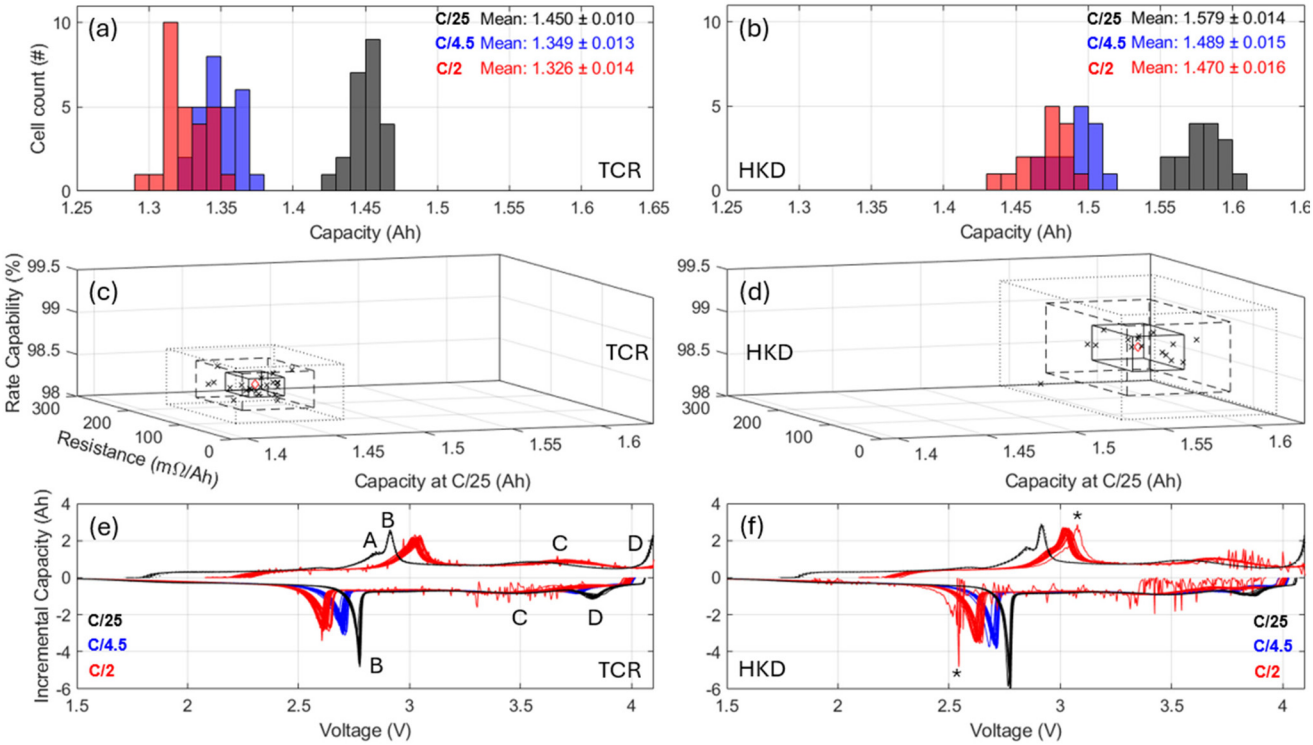

Fig. 1 (a and b) C/25, C/4.5, and C/2 capacity distributions. (c and d) Summary of the cell-to-cell variations. The inner square represents a 1σ spread, the dashed square 2σ, and the dotted one 3σ. (e and f) Incremental capacity for the C/25, C/4.5, and C/2 discharge, as well as the C/25 and C/2 charges. All for (a, c and f) the TCR and (b, d and f) the HKD cells.

dispersion in the studied parameters were comparable to that reported in Li-ion battery studies.[37]

Voltage response during cycling (Fig. 1e and f) serve as a sensitive indicator of cell-level reproducibility and reaction mechanisms. This comparison is easiest to visualize using a derivative curve such as incremental capacity (IC, $dQ/dV = f(V)$).[38] The differential capacity plots of the cells at C/25 (black curves in Fig. 1(e) and (f)), show four notable features. Starting at potentials near 2.75 V, a well-marked double peak during charge (A, B) for which one peak was visible during discharge (B), followed by a broad peak C, and a last peak D that is not completed at the charge cut-off, even for the lowest rates. Overall, the curves for all the cells overlap well except for one of the HKD cells, the cell with resistance outside of 2σ (* on Fig. 1(f)), which were noisy during the C/2 discharge but not during the subsequent C/4.5 and C/25 cycles. It is unclear if this noise and resistance from this cell are due to experimental error or inherent properties of the cell. The voltage response for both cells was identical, which suggested they have similar chemistries. Furthermore, their response matches data reported by Laufen and Klick *et al.*[14,17] and Bischof *et al.*,[15] which was expected as they used cells that matched the HKD cell chemistry. For a more detailed understanding of the peaks see Klick *et al.*'s study.[17] Given the apparent similarities in the cell behaviour and chemistry indicated by the RPT testing, it is not clear why the manufacturer specified upper voltage limit of the cells were different between the two batches of cells.

Materials characterization

Materials characterization was performed on electrode materials from an uncycled cell of each type. As this work is part of a larger study, the HKD was disassembled at 50% of its state of charge (SOC), whereas the TCR cell was disassembled at 0% SOC. This may have induced a difference between the two cells, which will be commented on when necessary.

SEM imaging of the cell electrodes is shown in Fig. 2. The PEs of the two cell types appear broadly similar, as seen in Fig. 2a and c. In both cases, flat surfaces were observed where the PE was pushed up against the separator with smaller boulder-like particles interspaced between the larger flat areas. One key difference observed is a potential film on the HKD PE. The HKD cell sample appear to have softer edges compared to clean ones for the TCR, which may suggest a film on the surface of the HKD PE that is not on the TCR PE. EDS (Fig. S3 and S4) and XPS (discussed later) did not show significant differences in the elemental composition of the surface, which may suggest that a CEI is formed on both PEs with a similar elemental composition. It is unclear if the NFM materials underwent a different manufacturing process which produced different particle morphologies observed in Fig. 2 or if there is a structural difference in the CEI film formed.

The NEs for both cells (Fig. 2b and d) also showed similar structures, with HC particles of various sizes compressed together and held with a binder. The primary difference

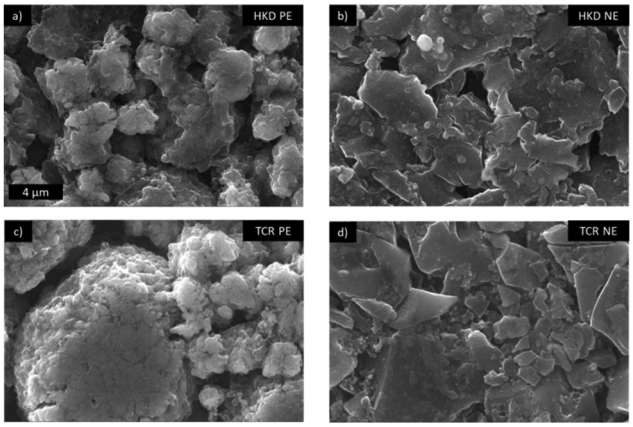

Fig. 2 SEM images of the electrodes of the HKD cells (a & b) and TCR cells (c & d). Images a and c show the PEs at 22.5 µm HFW and b and d show the NEs. All images have horizontal full width of 22.5 µm.

between the two was, again, the edges of the grains, with the edges of TCR HC (Fig. 2d) looking smoother than those of the HKD materials (Fig. 2b). This may, again, indicate a surface coating on the HKD material to manage the electrode/electrolyte interface better. This may also suggest that the HC material might have undergone different pyrolyzation/carbonization processes (including different precursors and processing temperatures), as the optimal configuration of amorphous carbon to graphite and pore size of HC is still being determined.[22,23,39]

The X-ray diffraction patterns shown in Fig. 3 indicate that the PEs for both cells contain $NaNi_{1/3}Fe_{1/3}Mn_{1/3}O_2$ (NFM111). Both PE materials exhibited the same hexagonal crystal structure in the $R\bar{3}m$ space group. Rietveld refinement showed similar lattice parameters with a = 2.96 Å, c = 16.13 Å for the TCR cell and a = 2.94 Å, c = 16.28 Å for the HKD one. Since these cells were disassembled at different states of charge, the slight differences in the lattice parameters may be due to changes in the Na content in the PE. Such shifts have been reported in the literature for layered metal oxides,[40–42] matching behaviour observed in Li-ion battery Ni-based electrodes.[43] To the best of our knowledge, this behaviour has not been related yet to SOC differences in the context of NIB materials. Despite the small shifts due to SOC differences, the presence of the same set of peaks confirms that the underlying materials are structurally the same.

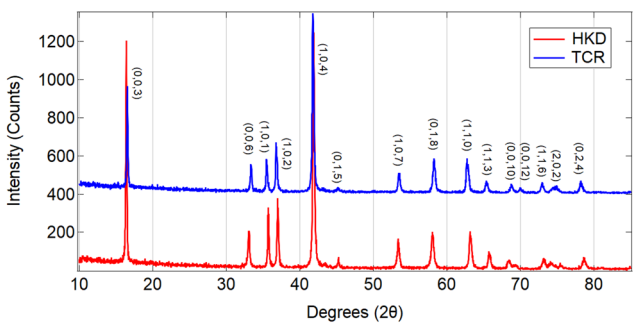

Fig. 3 XRD plots the HKD (red) and TCR (blue) positive electrodes. Note that the TCR cell had a 400 count offset applied to the pattern to improve clarity of the graph.

The NE of both cell types was determined to be HC, as indicated by the XRD patterns in Fig. 4 with two broad peaks corresponding to graphite observed in both NEs. The crystallite size for both was estimated to be on the order of 4 Å, suggesting the crystalline phases are nanocrystalline. The peaks' broadness also suggested a large amount of amorphous material. This matches well with reports on hard carbon materials, which are a mixture of crystalline graphite and amorphous carbon material.[23,39]

For the HKD cells, an additional peak is present which is assigned to Na_2C_2. This peak could indicate that, at 50% SOC, Na is bonding with the HC material in the NE likely *via* insertion into the carbon interlayers. Since it is well known that HC storage of Na^+ is complicated, with different mechanisms occurring depending on the type of HC and the SOC, this observation could be a valuable marker of what processes are occurring. This will be investigated further in future work.

Table 1 presents the composition of the PEs of uncycled HKD and TCR cells as determined from ICP-OES. Both cells showed a nearly identical composition of Fe, Mn, and Ni at relatively equal ratios for each element. This confirms that both cell PEs are NFM 111. Both also showed relatively close values of Na in the PE with the HKD cell showing a one percentage point increase in the weight of Na over the TCR cell which was unexpected as the HKD cell was disassembled at 50% SOC.

There are two potential reasons for the unusual trend in the Na concentration in the PE. First there could be increased Na loading in the PE to increase the capacity of the cell. Second, there could be increased Na salts (NaF *etc.*) in the electrolyte. These salts could have been left on the surface during

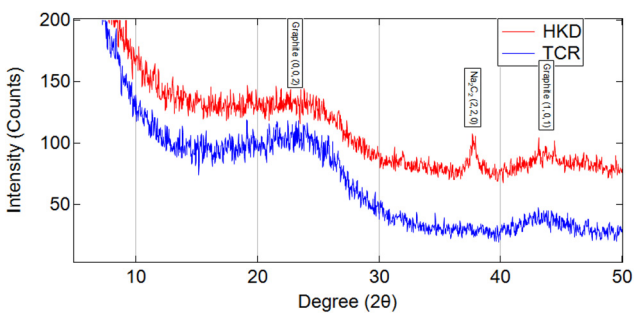

Fig. 4 XRD Plots of the HKD (blue) and TCR (red) negative electrodes.

Table 1 Weight percent of elements in the HKD and TCR PEs as determined by ICP-OES

	Na	Fe	Mn	Ni
HKD	17.33%	16.48%	16.59%	17.56%
TCR	16.7%	16.75%	16.1%	17.93%

analysis. When looking at the XPS of the PE in Fig. S5 we see that the signals for Na and F on the surface of the HKD sample is much higher than the TCR sample. Which lends some credence to increase NaF salt concentration in the electrolyte. However, when the cells were cycled to the same upper voltage limit of 4.1 V they showed a significant difference in capacity. With the TCR cell having 1.450 Ah *vs.* the HKD's 1.579 Ah this ~130 mAh of capacity change would suggest the HKD cell had an additional 0.159 g of Na ions to use during cycling in the PE. We suspect both increased NaF salt concentration and increased Na loading in the PE contributed to increased Na concentration observed.

While the additional Na ions could explain in part the increased capacity of the HKD cell, it would not account for the variation in the upper potential limit of 3.95 V (TCR) *vs.* 4.1 V (HKD). As mentioned in the introduction, cycling an NFM cell to 4.3 V or greater can cause an irreversible phase change[20] and, given the current youth of the NIB commercial production industry, this likely indicates that manufacturers do not yet have a standardized upper voltage limit with some being more conservative that others.

In order to look more indepth for differences between the two batches, the electrolyte was investigated *via* GC-MS, and the electrodes *via* XPS. The first significant difference between the cells was their respective electrolyte composition, Table 2. While both cells contained the same four constituent components: dimethyl carbonate (DMC), ethyl methyl carbonate (EMC), ethylene carbonate (EC), and propylene carbonate (PC), their ratios varied. The TCR electrolyte contained a majority of PC, while the HKD electrolyte had a more balanced mixture of the primary components. The remainder of the electrolyte composition consisted of trace materials likely added to enhance performance. Notably, the TCR electrolyte contained fewer trace components than the HKD cell. The primary components matched those used in Li-ion electrolyte compositions, suggesting that manufacturing processes from Li-ion technology may have been adapted for these cells.[44–46] Looking in more detail, the higher EC content in the HKD cells could indicate higher ionic conductivity as EC has been shown to have higher Na^+ conductivity than PC or DMC.[47] Furthermore, Chayambuka *et al.* found that increasing EC concentration increases Na^+ conductivity of an EC: PC binary mixture.[48] DMC and EMC mixed with PC have been shown to have a moderate impact on electrolyte conductivity and viscosity.[49] However, the literature currently has only considered binary mixtures of PC with some other component (EC, DMC, or EMC). The electrolytes observed here were composed of four different primary components with various trace components and it is unclear if results from the literature can be extrapolated to our study. Further study of the cell operation and electrolyte is required to determine how these different compositions will affect long-term cycling.

Table 2 GC-MS analysis of the weight percent of significant components of electrolytes used in the HKD and TCR cells

	DMC	EMC	EC	PC	Total
HKD	12.70%	14.30%	20.70%	46%	93.70%
TCR	17.60%	13.80%	13.60%	53.40%	98.40%

The second difference between the two cells was observed from XPS performed on the NEs, Fig. 5. The most apparent difference was the presence of C–F peaks in both the F 1s (689.9 eV) and C 1s (290.5 eV) regions for the TCR NEs, which, in combination with the peak at 287 eV, suggests polyvinylidene fluoride (PVDF) was used as the binder. The HKD NE spectra lacked the C–F peak in either the F 1s or C 1s regions, implying that PVDF was not used as a binder, with SBR being the most likely replacement, as it was listed in the SDS. Both PVDF and non-fluorinated polymers are commonly used in both Li and Na batteries to hold the active material together during cycling.[50,51] PVDF is less flexible than SBR and does not respond as well to significant volume changes during cycling as other polymers.[52] This would suggest that the HKD cells could have longer cycle life due to a more resilient NE.

XPS experiments also suggested differences in the initial SEI on the NEs as differences existed in the C 1s, S 2p, O 1s, and Na 1s regions, Fig. 5. While the HKD NE spectra have no peaks corresponding to PVDF, there is a small carbide peak at 283.6 eV, which was not present in the TCR NE. The O 1s peak for the TCR NE spectrum was at a higher binding energy than for the HKD NE, suggesting a difference in the composition of O-containing compounds. The other distinct difference in the SEI was in the S content. The HKD NE spectrum not only has a larger quantity of sulfur (~1 at% *vs.* <0.5 at%), but that sulfur is in a more reduced form, as shown in Fig. 5d. S-containing compounds are reported as film-forming additives in Na batteries, which are consumed during the initial cycle and would not appear in an electrolyte analysis.[53] Overall, this suggests the composition of the SEI is different for the TCR and HKD cells. Current theory on SEI of NIBs is that inorganic-based SEIs are more stable and Na^+ conductive. The presence of S compounds in the HKD SEI may also influence the stability of the SEI suggesting that the HKD may have a more stable SEI and may perform better during cycling.[54] Additionally, the O 1s spectrum for the TCR electrode has a shoulder at 533.9 eV, which may correspond to adsorbed water.[55] Water contamination in the cells is linked to the generation of HF, which leads to a less stable SEI.[56,57]

The final difference between the cells is in the average oxidation state of the Na compounds (Fig. 5e). There is a 0.5 eV difference in the Na 1s peak position (1072.5 eV for TCR and 1072.0 eV for HKD), suggesting the Na containing compounds in the HKD electrode were more reduced. This could also be due to the different states of charge of the anodes. Because it is challenging to assign Na compounds based only on the Na 1s peak position, the Na KLL Auger peak was measured as well, and the modified Auger parameter was calculated to be 2060.8 eV for TCR and 2061.3 eV for HKD, both consistent with ionic Na compounds other than NaF.[55,58]

The PEs were also compared using XPS; however, minimal differences were found between the HKD and TCR cells (Fig. S8).

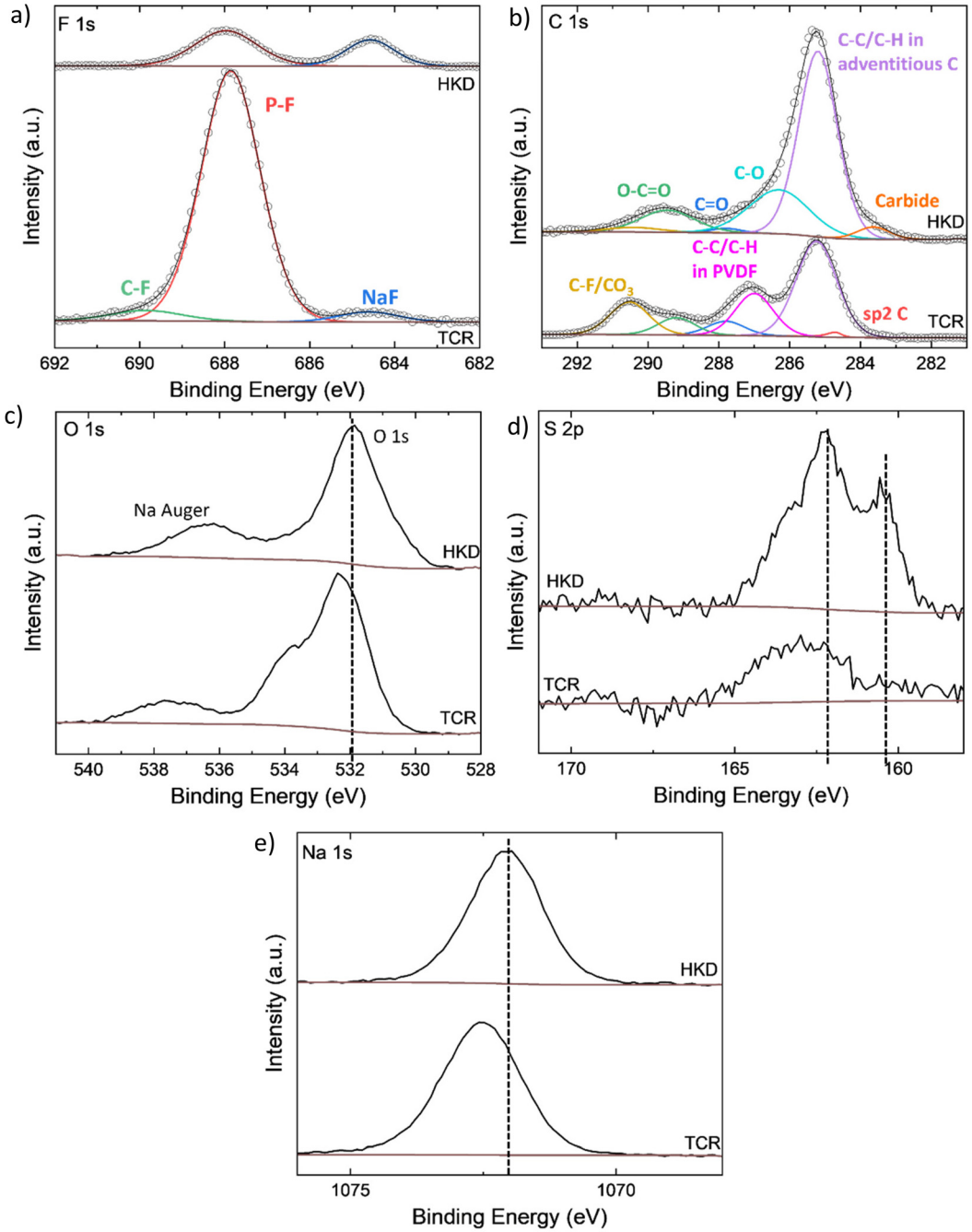

Fig. 5 High resolution analysis-ray photoelectron spectra of elements of interest in the HKD and TCR NEs. (a) F 1s region, (b) binding 1s region, (c) binding 1s region, (d) S 2p region, and (e) Na 1s region.

The NEs and PEs of both cells contain P originating from $NaPF_6$ salt (137.8 eV) as well as from phosphates and/or phosphites, Fig. S5, based on the P $2p_{3/2}$ peaks at 133.6 eV and 135.5 eV.[55,58] Various phosphates and other P containing compounds are commonly used as flame retarding additives in NIBs.[53] For both cells, the F 1s region shows peaks corresponding to metal fluorides, P–F, from the salt, and C–F, likely from PVDF. Unlike the NEs, the Na in the PEs appears to be the same in both cells with an asymmetric Na 1s peak that has components at 1071.5 eV and 1073 eV and a modified Auger parameter of 2059.9 eV, matching NaF.[55,58] The most significant difference between the TCR and HKD PEs is in the O 1s region, where the O 1s peak for the TCR cell is shifted to higher binding energy relative to the O 1s peak for the HKD cell. Peak fitting of this region is complicated by the presence of a Na Auger peak at 538 eV, thus we cannot make definitive conclusions here.

Table 3 provides a direct comparison of the core differences between the cells from their manufacturer data sheet and the

Table 3 Summary of the key differences between cell type

Feature	HKD	TCR
Upper voltage limit (V)	4.1	3.95
1C current (A)	1.5	1.3
EC in electrolyte (wt%)	20.7%	13.6
NE binder	SBR	PVDF
Water present	No	Yes
SEI composition	More inorganic components	Less inorganic components

materials characterization work done on them. On their face these cells appeared very similar with near identical PE and NE compositions and structures. Looking at the data we see they have distinct operational differences prescribed by their respective manufacturers. We see the HKD cells have a higher upper voltage and 1C current than the TCR cells. This would lead to higher potential capacities and power for the HKD cells during operation.

On a materials level the HKD cells would appear to be well suited for cycling based on the prevailing scientific consensus. There is more EC in the electrolyte which is thought to increase Na^+ transport rate. The TCR cells use a binder that is more rigid than the HKD cells, suggesting that over cycling as the NE expands and contracts the HKD NE may perform better. The HKD cells did not have water present in their NE while the TCR cells did. Water can lead to significant side reactions like HF formation which can degrade the cell significantly during cycling. Finally, the TCR cell's SEI is thought to be less stable than the HKD cell's SEI, where the greater amount of inorganic compounds is thought to increase stability. All of this suggests that the HKD cells should have longer cycle life with greater capacity than their TCR counter parts.

Initial cycling results

Fig. 6 presents the initial cycling data for the HKD and TCR cells cycled at 25 °C through their full SOC range as determined by voltage and at a C-rate of 0.5C for both charging and discharging. By 350 cycles both cells are below 80% of their initial capacity. This is about an order of magnitude less than what was indicated in the manufacturer's data sheet under these cycling conditions. As of this writing only one study has been published on cycling of NFM/hard carbon which showed cells above 80% capacity for at least 1500 cycles.[17] This discrepancy suggests that there may be significant variability in the quality of commercial cells with nominally identical chemistries, depending on the manufacturer and production standards.

Furthermore, the cells showcased significantly different degradation rates under the same conditions. The TCR cells showed relatively linear decay throughout their cycling with two rates of fade, a relatively flat one for the first 150 cycles then a slight increase in slope down to 80% capacity for the last 150 cycles. The HKD cells showed a steeper initial linear decay a much more marked acceleration after 100 cycles with a well-defined knee. One cell experiences a knee but "only" decayed to 40% capacity by the end of cycling. Both cells

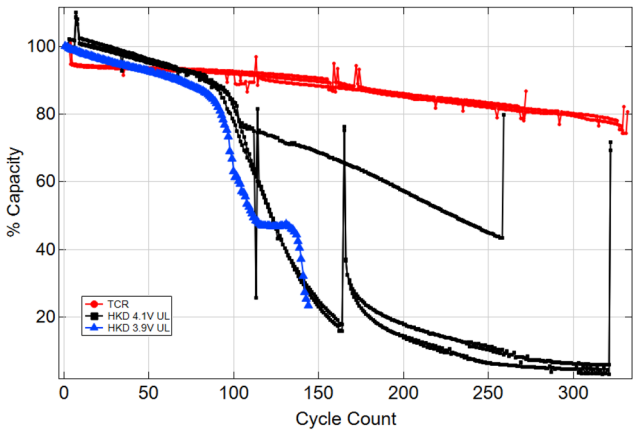

Fig. 6 Initial cycling data of TCR (red) and HKD (black and blue) cells cycled at 0.5C/0.5C, through a SOC range of 0–100%. TCR and HKD cells cycled to 4.1 V (black) were cycled in 25 °C temperature chamber. HKD cells cycled to 3.9 V (blue) were cycled at 20 °C.

appear to recover some capacity during the RPT test that was conducted between cycles to evaluate performance. In the HKD cells, this recovery is short-lived, and the cells quickly return to their previous capacity values.

Fig. 7 shows initial incremental capacity analysis of HKD and TCR cells during the initial cycling shown in Fig. 6. While the cells were cycled in their duty cycles at the suggested upper voltage limit from each manufacturing specification sheet the ICA cycling was conducted at C/25 to an upper voltage of 4.1 V to create a true comparison of performance across a voltage region. What we notice immediately is that above 4 V the HKD Ah/V values become very unstable suggesting that there are parasitic side reactions occurring in this region. The TCR cells appear stable in this region.

The HKD cells degradation was dominated by the loss of sodium inventory (LSI) as shown by the significant reduction in the peak hight near 2.75 V and in the decrease in values for the region between 3 and 4 V. The TCR cells showed LSI occurred as well through reductions in values in the charge and discharge curves between 3 and 4 V. The peaks near 2.75 V show shifts that indicate both loss of active material (LAM) at the PE and NE occurred as well.

Through this comparison of initial cycling performance data, we can potentially see the influence of materials and performance markers previously noted in two ways. First is the consistency of the cell performance. Overall, the HKD cells showed more variation in performance across all the initially evaluated cycling markers (Fig. 1) while the TCR cells were much closer to each other. This translates to the cycling data, where one HKD cell differed significantly in performance from the other two, and the other two show some variations in capacity fade rates during cycling. The TCR cells, however, remained relatively close to each other and had trends that occurred at the same time and at the same relative magnitude.

Second, there was an impact of the different manufacturing and operational choices. There are three possible contributors

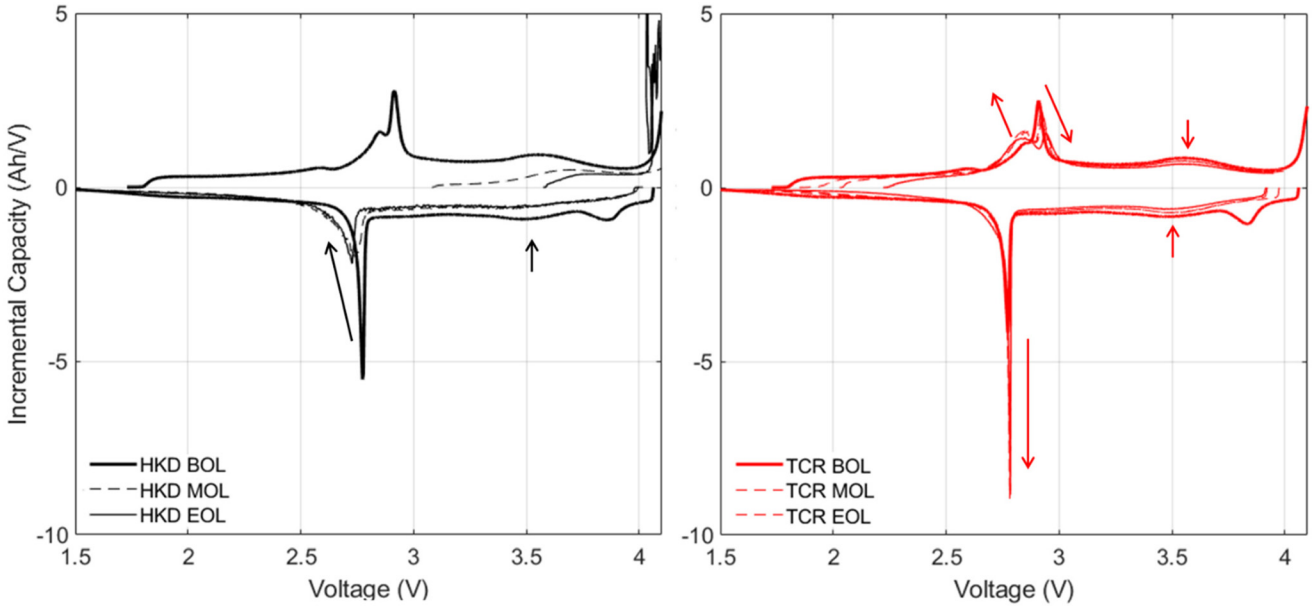

Fig. 7 Incremental capacity analysis (ICA) of the HKD and TCR cells during cycling.

to this issue. First is the voltage difference. As mentioned before, there is a 150 mV difference in the upper voltage limit of the two cells. Voltages of 4.3 V have been associated with degradation of the NFM material.[20,21] The degradation described may be occurring in the HKD cells with the higher voltage limit. Recent work by Bischof *et al.* suggested that lowering upper voltage limits would also reduce the amount of Na-plating that would occur in the cell.[58] In this work they used the same HKD cells that we used in this study. They found that cycle life could be extended significantly by reducing upper voltage limits from 4.1 V to 3.9 V.

We explored the possibility of side reactions impacting the HKD cells at the higher upper voltage limit. Fig. 6 shows capacity fade data for a HKD cell cycled with an upper limit of 3.9 V (blue) which showed similar if slightly worse performance when compared to the HKD cells cycled at 4.1 V. Notably this cell was cycled at 5 °C lower than the other cells in this cycling study which according to Waldmann *et al*. would not make a significant different in cell performance.[59] Our results for cycling at a lower voltage limit conflict with results from Bischof *et al*. who showed an improvement of cycle life by decreasing the upper voltage limit of their HKD type cells.[58] Though we do see similar trends in cycling with a sharp knee point near 100 cycles that correlates to a significant loss in efficiency suggesting we are seeing similar phenomenon broadly during cycling. The results shown in Fig. 6 also disputes the theory that we are observing a phase change in the PE at higher voltages as there was not significant change between our cells cycled at 4.1 V and 3.9 V. So, voltage control in this case does not seem to be the issue.

The main difference in cell performance here appears to be the type of degradation mechanisms that occurring during cycling. As noted earlier we observed parasitic side reactions with LSI in the HKD cells and some LSI plus LAM at PE and NE in the TCR cells. Which would suggest there is something in the HKD cells that enabled increased Na-plating that caused the rapid cell failure.

In theory, the HKD cells used a NE binder that is more resistant to volumetric changes, making it less likely that the difference in binder is the cause for the more rapid capacity fade. The electrolyte composition and the initial SEI could also have played a role as EC and inorganic sulfur, that are thought to improve performance, were found in higher quantities in the HKD cells (Table 2 and Fig. 5d). Additionally, the TCR cell had signs of water at the NE, which may have indicated contamination during assembly. It seems that these materials factors were not as important as we thought from a review literature on Na-ion batteries. It is currently unclear to us why the TCR has a more stable cycling profile than the HKD cells. This highlights the need for further work to understand how a whole Na-ion battery operates and what are the crucial factors to optimize.

Conclusions

Our initial survey of two NIB cell types shows manufacturing consistency within batches that approach commercial Li-ion production. This suggests that the manufacturing consistency of these NIB cells approaches established Li-ion battery production, indicating a relatively mature fabrication process. This is likely due to the fact that NIB materials can be processed using the same production techniques as Li-ion. The initial cycling data showed that these cells significantly underperform their advertised cycle life by about an order of magnitude. The HKD cells did much worse than the TCR cells, but both types are below 80% after 300 cycles.

Additional characterization of the two cell types revealed differences that may explain the poor initial performance. First, they have different upper voltage limits, which may have induced higher degradation of the NFM material in the HKD cells and increase Na-plating. The HKD cells also appear to contain more Na^+ ions than the TCR cells. Other core differences in both cells lie in the composition of the electrolyte and the binder used in the NE materials. The changes in the electrolyte point to differences in the initial SEI observed *via* XPS. However, the differences in the SEI and binder did not explain the poor cycling performance of the HKD cells.

Cycling the HKD cells at lower upper voltage limit did not significantly change performance of the HKD cells which showed a knee point near 100 cycles in both conditions. This disagrees with initial literature indicating that reduced upper voltage limit reduced Na-plating and increased cycle life. This would also indicate we are not seeing a phase change in the PE either. Rather there appears to be something inherent to the HKD cells that promotes increase Na-plating and other parasitic side reactions. This is observed in our ICA analysis (Fig. 7) where the TCR cells showed much less LSI and no parasitic reactions occurring.

Overall, our study indicates that there is a significant variation in the quality of available commercial Na-ion batteries, and manufacturers have not agreed on set performance metrics for their cells. This study highlights the need for standardized testing of newly commercialized cells, such as done so above, to validate and understand cell variance, reliability, and degradation modes. Further work will be conducted to understand the origins of cell degradation in the present cells to inform how to improve future generations of NIBs.

Experimental

Procurement and cycle testing

For this study, one hundred and fifty 18650 format NIB cells were purchased from Shenzhen Mushang Electronics, labeled Hakadi, and Guangzhou Tycorun Energy, labelled Tycorun (Table S1). Electrochemical testing was carried out using Arbin SCTS battery testers with cells placed into commercially available 18650 battery holders in SPX Tenney Model T10C-1.5 environmental chambers set at 25 °C. All Cells were initially cycled six times at a rate of C/2 to ensure they had stabilized. The cells were then cycled according to the RPT protocol proposed in ref. 20 with cycles at C/4.5 and C/25 with C/50 trickle charge steps.

Materials characterization was conducted on uncycled cells disassembled in an argon-filled glove box using 18650 format Li-ion disassembly procedures.[21–23] The HKD cells were disassembled at 50% state of charge (SOC). The TCR cells were disassembled at 0% SOC. All electrode characterizations were done on unwashed samples, without any surface modifications. X-ray diffraction (XRD), scanning electron microscopy (SEM), gas chromatography mass spectrometry (GC-MS), inductively coupled plasma mass spectrometry/optical emission spectroscopy (ICP-MS/OES), and X-ray photoelectron spectroscopy (XPS) were conducted on the PE and NE of each cell. Full details of the materials characterization work can be found in the SI. The difference in SOC should only impact the comparison of the NE XRD pattern and Na content in ICP-OES of the electrodes considered here.

ICP-GCMS

Organic component analysis was performed on chemical extracts of swab samples *via* liquid injection on an Agilent 6890N gas chromatograph, coupled with an Agilent 5973 Network Mass Selective Detector. Samples were prepared by diluting 5 μL of electrolyte in 1 mL of ethanol. The gas chromatography mass spectrometry (GC-MS) analysis was carried out in split mode 50 : 1, with separation on a Restek Rxi-5 ms column (60 m × 0.25 μm, 0.32 mm ID). The inlet and MS transfer line were both kept at 300 °C. The helium carrier gas was kept at a constant flow of 1.6 mL min^{-1}. The GC oven temperature program was 40 °C for 1 min, ramped to 200 °C at 7 °C min^{-1}, followed by ramping to 300 °C at 15 °C min^{-1}. Acquisition was performed in the mass range of 15–550 *m*/*z*.

SEM imaging was performed using a ZEISS EVO SEM. The beam strength for imaging was set to 20 kV.

X-ray photoelectron spectroscopy (XPS). Measurements were taken on a Kratos AXIS Supra XPS operated at a base pressure lower than 5×10^{-9} torr, using a monochromatic Al Kα X-ray source ($h\nu$ = 1486.6 eV). Surveys and high-resolution scans for elements of interest were taken for each sample. Spectra were obtained using a large analyzer spot size and a pass energy of 160 eV for all surveys and 20 eV for the high-resolution scans, with a step size of 1 eV for the surveys and 0.1 eV for the high resolution scans. Charge compensation was done using a charge neutralizer with a filament current of 0.42 A.

X-ray diffraction. XRD was done using a Rigaku SmartLab X-ray Diffractometer with electrode powder scraped from the current collector. The characterization was done in the open air on a single-crystal silicon no-background sample stage. The instrument used a beam strength of 40 kV and 44 mA with a CuKα source. Data was collected in parallel beam mode using a 2θ scan procedure with a theta = 7° offset. The scan range was 2θ = 10 to 80° with a step size of 0.04° and a rate of 5° min^{-1}. XRD patterns were analyzed using the PDXL software from Rigaku. The data were fit to known patterns in the database, and lattice spacing and crystal size were determined by the PDXL program using the Rietveld refinement method.

Inductively coupled plasma mass spectrometry/optical emission spectroscopy (ICP-MS/OES). A Mars 6 (CEM Corporation) extraction system equipped with polytetrafluoroethylene (PTFE) vessels was used in the digestion of the samples. The microwave digestions in the PTFE vessels were carried out in multiple steps, with the first consisting of the addition of sulfuric acid (10 ml) to 0.3 g of sample. These samples were heated for 0.5 h until they reached a temperature of 260 °C (maximum microwave power, 1800 W) and held at that temperature for 0.25 h. Samples were allowed to cool and depressurized. This heating cycle was repeated four additional times.

Following the fifth cooling and depressurization, nitric acid (10 ml) was added to the Teflon vessel, and a microwave digestion cycle was completed as follows: 0.5 h ramp to 210 °C (maximum microwave power, 1800 W) followed by a hold at that temperature for 15 min. Sample digests were then diluted to 50 mL.

Author contributions

Conceptualization: RMW, DA, MD; writing – original draft: RMW, DA, MD, MLM; writing – review and editing: RMW, DA, MD, MLM, AB, LTC; investigation: CR, MLM, JL, MR, NV, JRK, DS, BJ, RMW; formal analysis: RMW, MLM, DA, DB, EEV, VMG, IC; funding acquisition: RMW, LTC, AB, DA, MD; project administration: RMW, DA, MD.

Conflicts of interest

There are no conflicts to declare.

Data availability

Raw data files for the materials characterization (SEM, XRD, ICP-OES, XPS *etc.*) data will be provided at https://www.sandia.gov/ess/tools-resources/rd-data-repository.

Cycling data will be available upon request to the corresponding authors as this is part of a on going study.

Supplementary information (SI) is available. See DOI: https://doi.org/10.1039/d5eb00161g.

Acknowledgements

M. D. is thankful for funding from ONR under grant number # N00014-21-1-2250.

This material is based upon work supported by the U.S. Department of Energy, Office of Electricity (OE), Energy Storage (R. M. W., C. R., A. B., L. T. C., M. L. M., J. K., B. J., M. R., N. R., D. S. and J. L.).

D. A. acknowledges funding from the Spanish Ministry of Science, Innovation and Universities under grant PID2022-141792OB-I00, and from the Principality of Asturias under grant IDE/2024/000769.

I.C. acknowledges funding from the Spanish Ministry of Science, Innovation and Universities under grant PID2023-147151OB-I00, and from the Principality of Asturias under grant IDE/2024/000749.

Sandia National Laboratories is a multisession laboratory managed and operated by National Technology & Engineering Solutions of Sandia, LLC, a wholly-owned subsidiary of Honeywell International, Inc., for the US DOE's National Nuclear Security Administration under contract DE-NA-0003525. The views expressed in the article do not necessarily represent the views of the US DOE or the United States Government.

References

1 N. Tapia-Ruiz, A. R. Armstrong, H. Alptekin, M. A. Amores, H. T. Au, J. Barker, R. Boston, W. R. Brant, J. M. Brittain, Y. Chen, M. Chhowalla, Y. S. Choi, S. I. R. Costa, M. C. Ribadeneyra, S. A. Cussen, E. J. Cussen, W. I. F. David, A. Desai, S. A. M. Dickson, E. Eweka, J. D. Forero-Saboya, C. P. Grey, J. M. Griffin, P. Gross, X. Hua, J. T. S. Irvine, P. Johansson, M. O. Jones, M. Karlsmo, E. Kendrick, E. Kim, O. Kolosov, Z. N. Li, S. F. L. Mertens, R. Mogensen, L. Monconduit, R. E. Morris, A. J. Naylor, S. Nikman, C. A. O'Keefe, D. M. C. Ould, R. G. Palgrave, P. Poizot, A. Ponrouch, S. Renault, E. M. Reynolds, A. Rudola, R. Sayers, D. O. Scanlon, S. Sen, V. R. Seymour, B. Silván, M. T. Sougrati, L. Stievano, G. S. Stone, C. Thomas, M. M. Titirici, J. C. Tong, T. J. Wood, D. S. Wright and R. Younesi, *J. Phys.: Energy*, 2021, **3**, 031503, DOI: 10.1088/2515-7655/ac01ef.

2 T. Perveen, M. Siddiq, N. Shahzad, R. Ihsan, A. Ahmad and M. I. Shahzad, *Renewable Sustainable Energy Rev.*, 2020, **119**, 109549, DOI: 10.1016/j.rser.2019.109549.

3 K. Chayambuka, G. Mulder, D. L. Danilov and P. H. L. Notten, *Adv. Energy Mater.*, 2020, **10**, 2001310, DOI: 10.1002/aenm.202001310.

4 K. M. Abraham, *ACS Energy Lett.*, 2020, **5**, 3544–3547, DOI: 10.1021/acsenergylett.0c02181.

5 J. F. Peters, A. P. Cruz and M. Weil, *Batteries*, 2019, **5**, 10, DOI: 10.3390/batteries5010010.

6 J. M. Tarascon, *Joule*, 2020, **4**, 1616–1620, DOI: 10.1016/j.joule.2020.06.003.

7 A. Rudola, A. J. R. Rennie, R. Heap, S. S. Meysami, A. Lowbridge, F. Mazzali, R. Sayers, C. J. Wright and J. Barker, *J. Mater. Chem. A*, 2021, **9**, 8279–8302, DOI: 10.1039/d1ta00376c.

8 L. U. Subasinghe, G. S. Reddy, A. Rudola and P. Balaya, *J. Electrochem. Soc.*, 2020, **167**, 110504, DOI: 10.1149/1945-7111/ab9ee9.

9 L. H. B. Nguyen, P. S. Camacho, J. Fondard, D. Carlier, L. Croguennec, M. R. Palacin, A. Ponrouch, C. Courrèges, R. Dedryvère, K. Trad, C. Jordy, S. Genies, Y. Reynier and L. Simonin, *J. Power Sources*, 2022, **529**, 231253, DOI: 10.1016/j.jpowsour.2022.231253.

10 H. Hijazi, Z. W. Ye, L. B. Zhang, J. Deshmukh, M. B. Johnson, J. R. Dahn and M. Metzger, *J. Electrochem. Soc.*, 2023, **170**, 070512, DOI: 10.1149/1945-7111/ace4fa.

11 M. L. He, R. Davis, D. Chartouni, M. Johnson, M. Abplanalp, P. Troendle and R. P. Suetterlin, *J. Power Sources*, 2022, **548**, 232036, DOI: 10.1016/j.jpowsour.2022.232036.

12 M. L. He, A. E. L. Mejdoubi, D. Chartouni, M. Morcrette, P. Troendle and R. Castiglioni, *J. Power Sources*, 2023, **588**, 233741, DOI: 10.1016/j.jpowsour.2023.233741.

13 J. Q. Huang, L. A. Blanquer, J. Bonefacino, E. R. Logan, D. A. Dalla Corte, C. Delacourt, B. M. Gallant, S. T. Boles, J. R. Dahn, H. Y. Tam and J. M. Tarascon, *Nat. Energy*, 2020, **5**, 674–683, DOI: 10.1038/s41560-020-0665-y.
14 H. Laufen, S. Klick, H. Ditler, K. L. Quade, A. Mikitisin, A. Blömeke, M. Schütte, D. Wasylowski, M. Sonnet, L. Henrich, A. Schwedt, G. Stahl, F. Ringbeck, J. Mayer and D. U. Sauer, *Cell Rep. Phys. Sci.*, 2024, **5**, 101945, DOI: 10.1016/j.xcrp.2024.101945.
15 K. Bischof, V. Marangon, M. Kasper, A. Aracil Regalado, M. Wohlfahrt-Mehrens, M. Hölzle, D. Bresser and T. Waldmann, *J. Power Sources Adv.*, 2024, **27**, 100148, DOI: 10.1016/j.powera.2024.100148.
16 P. Rodríguez-Iturriaga, S. Thatipamula and S. Onori, *Future Batteries*, 2025, **6**, 100056, DOI: 10.1016/j.fub.2025.100056.
17 S. Klick, H. Laufen, M. Schütte, B. W. Qian, K. L. Quade, C. Rahe, M. Dubarry and D. U. Sauer, *Batteries Supercaps*, 2025, **8**, e202400546, DOI: 10.1002/batt.202400546.
18 G. Gupta, B. Satola, L. Komsiyska, C. Harms, T. Hickmann and A. Dyck, *J. Electrochem. Soc.*, 2022, **169**, 080503, DOI: 10.1149/1945-7111/ac8240.
19 D. Kim, E. Lee, M. Slater, W. Lu, S. Rood and C. S. Johnson, *Electrochem. Commun.*, 2012, **18**, 66–69, DOI: 10.1016/j.elecom.2012.02.020.
20 V. Duffort, E. Talaie, R. Black and L. F. Nazar, *Chem. Mater.*, 2015, **27**, 2515–2524, DOI: 10.1021/acs.chemmater.5b00097.
21 Y. Xie, H. Wang, G. Xu, J. Wang, H. Sheng, Z. Chen, Y. Ren, C. J. Sun, J. Wen, J. Wang, D. J. Miller, J. Lu, K. Amine and Z. F. Ma, *Adv. Energy Mater.*, 2016, **6**, 1601306, DOI: 10.1002/aenm.201601306.
22 L. Kalder, A. Olgo, J. Luehrs, T. Romann, R. Harmas, J. Aruvali, P. Partovi-Azar, A. Petzold, E. Lust and E. Hark, *Energy Storage Mater.*, 2024, **67**, 103272, DOI: 10.1016/j.ensm.2024.103272.
23 F. N. Shafiee, S. A. Mohd Noor, M. A. A. Mohd Abdah, S. H. Jamal and A. Samsuri, *Heliyon*, 2024, **10**, e29512, DOI: 10.1016/j.heliyon.2024.e29512.
24 K. Bhawana, M. Gautam, G. K. Mishra, N. Chakrabarty, S. Wajhal, D. Kumar, D. P. Dutta and S. Mitra, *Carbon*, 2023, **214**, 118319, DOI: 10.1016/j.carbon.2023.118319.
25 S. Altundag, S. Altin, S. Yasar and E. Altin, *Vacuum*, 2023, **210**, 111853, DOI: 10.1016/j.vacuum.2023.111853.
26 C. Y. Zhao, Y. W. Wei, Y. Pan and C. H. Chen, *Solid State Ionics*, 2024, **412**, 116586, DOI: 10.1016/j.ssi.2024.116586.
27 B. Karaman, H. Tonnoir, D. Huo, B. Carré, A. F. Léonard, J. C. Gutiérrez, M. L. Piedboeuf, A. Celzard, V. Fierro, C. Davoisne, R. Janot and N. Job, *Carbon*, 2024, **225**, 119077, DOI: 10.1016/j.carbon.2024.119077.
28 X. X. Fu, M. Yang, M. H. Zhai, C. Zhang, H. J. Niu and Y. Q. Li, *Energy Storage Mater.*, 2024, **70**, 103450, DOI: 10.1016/j.ensm.2024.103450.
29 F. Li, Z. Sun, M. Dong, M. Gong and P. Hou, *Chem. Eng. J.*, 2024, **480**, 147940, DOI: 10.1016/j.cej.2023.147940.
30 J. Y. Zhang, J. J. Gai, K. M. Song and W. H. Chen, *Cell Rep. Phys. Sci.*, 2022, **3**, 100868, DOI: 10.1016/j.xcrp.2022.100868.
31 D. X. Ouyang, K. Wang, Y. M. Pang and Z. R. Wang, *ACS Appl. Energy Mater.*, 2023, **6**, 2063–2071, DOI: 10.1021/acsaem.2c04081.
32 K. Rumpf, M. Naumann and A. Jossen, *J. Energy Storage*, 2017, **14**, 224–243, DOI: 10.1016/j.est.2017.09.010.
33 M. Dubarry, N. Vuillaume and B. Y. Liaw, *Int. J. Energy Res.*, 2010, **34**, 216–231, DOI: 10.1002/er.1668.
34 Y. Preger, J. Mueller, A. Fresquez, S. Allu and C. Rich, *J. Electrochem. Soc.*, 2025, **172**, 050540, DOI: 10.1149/1945-7111/add777.
35 M. Dubarry and G. Baure, *Electronics*, 2020, **9**, 152, DOI: 10.3390/electronics9010152.
36 A. Devie and M. Dubarry, *Batteries*, 2016, **2**, 28, DOI: 10.3390/batteries2030028.
37 A. Devie, G. Baure and M. Dubarry, *Energies*, 2018, **11**, 1031, DOI: 10.3390/en11051031.
38 M. Dubarry and D. Anseán, *Front. Energy Res.*, 2022, **10**, 1023555, DOI: 10.3389/fenrg.2022.1023555.
39 M. J. Xiao, X. H. Dai and Y. Jiang, *J. Energy Storage*, 2025, **111**, 115411, DOI: 10.1016/j.est.2025.115411.
40 S. Komaba, N. Yabuuchi, T. Nakayama, A. Ogata, T. Ishikawa and I. Nakai, *Inorg. Chem.*, 2012, **51**, 6211–6220, DOI: 10.1021/ic300357d.
41 M. Xu, D. G. Ivey, Z. Xie and W. Qu, *J. Power Sources*, 2015, **283**, 358–371, DOI: 10.1016/j.jpowsour.2015.02.114.
42 X.-M. Lin, X.-T. Yang, H.-N. Chen, Y.-L. Deng, W.-H. Chen, J.-C. Dong, Y.-M. Wei and J.-F. Li, *J. Energy Chem.*, 2023, **76**, 146–164, DOI: 10.1016/j.jechem.2022.09.016.
43 J. Li, J. Harlow, N. Stakheiko, N. Zhang, J. Paulsen and J. Dahn, *J. Electrochem. Soc.*, 2018, **165**, A2682–A2695, DOI: 10.1149/2.0491811jes.
44 J. Deng, W. Yang, Y. N. Zhang, L. N. Pan, F. R. Kang, X. Ji and H. Y. Wu, *J. Energy Storage*, 2025, **110**, 115308, DOI: 10.1016/j.est.2025.115308.
45 M. Marcinek, J. Syzdek, M. Marczewski, M. Piszcz, L. Niedzicki, M. Kalita, A. Plewa-Marczewska, A. Bitner, P. Wieczorek, T. Trzeciak, M. Kasprzyk, P. Łężak, Z. Zukowska, A. Zalewska and W. Wieczorek, *Solid State Ionics*, 2015, **276**, 107–126, DOI: 10.1016/j.ssi.2015.02.006.
46 P. Verma, P. Maire and P. Novák, *Electrochim. Acta*, 2010, **55**, 6332–6341, DOI: 10.1016/j.electacta.2010.05.072.
47 A. K. Giri and H. Oberhofer, *J. Mol. Liq.*, 2024, **413**, 125920, DOI: 10.1016/j.molliq.2024.125920.
48 K. Chayambuka, R. Cardinaels, K. L. Gering, L. Raijmakers, G. Mulder, D. L. Danilov and P. H. L. Notten, *J. Power Sources*, 2021, **516**, 230658, DOI: 10.1016/j.jpowsour.2021.230658.
49 A. Hofmann, Z. Q. Wang, S. P. Bautista, M. Weil, F. Müller, R. Löwe, L. Schneider, I. U. Mohsin and T. Hanemann, *Electrochim. Acta*, 2022, **403**, 139670, DOI: 10.1016/j.electacta.2021.139670.
50 R. R. Li, Z. Yang, X. X. He, X. H. Liu, H. Zhang, Y. Gao, Y. Qiao, L. Li and S. L. Chou, *Chem. Commun.*, 2021, **57**, 12406–12416, DOI: 10.1039/d1cc04563f.

51 W. J. Zhang, M. Dahbi and S. Komaba, *Curr. Opin. Chem. Eng.*, 2016, **13**, 36–44, DOI: 10.1016/j.coche.2016.08.001.
52 R. Wang, L. Feng, W. Yang, Y. Zhang, Y. Zhang, W. Bai, B. Liu, W. Zhang, Y. Chuan, Z. Zheng and H. Guan, *Nanoscale Res. Lett.*, 2017, **12**, 575, DOI: 10.1186/s11671-017-2348-6.
53 J. Zhang, J. Li, H. Wang and M. Wang, *Front. Chem.*, 2023, **11**, 1253959, DOI: 10.3389/fchem.2023.1253959.
54 H. Y. Che, X. R. Yang, H. Wang, X. Z. Liao, S. S. Zhang, C. S. Wang and Z. F. Ma, *J. Power Sources*, 2018, **407**, 173–179, DOI: 10.1016/j.jpowsour.2018.08.025.
55 A. Y. Lee, C. J. Powell, J. M. Gorham, A. Morey, J. H. J. Scott and R. J. Hanisch, *Data Sci. J.*, 2024, **23**, 45, DOI: 10.5334/dsj-2024-045.
56 K. Hankins, M. H. Putra, J. Wagner-Henke, A. Gross and U. Krewer, *Adv. Energy Mater.*, 2024, 2401153, DOI: 10.1002/aenm.202401153.
57 P. Barnes, K. Smith, R. Parrish, C. Jones, P. Skinner, E. Storch, Q. White, C. J. Deng, D. Karsann, M. L. Lau, J. J. Dumais, E. J. Dufek and H. Xiong, *J. Power Sources*, 2020, **447**, 227363, DOI: 10.1016/j.jpowsour.2019.227363.
58 K. Bischof, M. Feinauer, A. A. Regalado, M. Wohlfahrt-Mehrens, M. Hölzle and T. Waldmann, *J. Electrochem. Soc.*, 2025, **172**, 090520, DOI: 10.1149/1945-7111/ae0075.
59 T. Waldmann, A. Aracil-Regalado, K. Bischof, M. Wohlfahrt-Mehrens and M. Hölzle, *J. Electrochem. Soc.*, 2025, **172**, 100514, DOI: 10.1149/1945-7111/ae0d07.